Electronic Supplementary Material (ESI) for ChemComm.

Ion Mobility Separation of Deprotonated Oligosaccharide Isomers - Evidence for Gas-Phase Charge Migration

W. B. Struwe,[a]† C. Baldauf[b]*, J. Hofmann,[b] P. M. Rudd[a] and K. Pagel[b,c]*

[a] *National Institute of Bioprocessing, Research and Training (NIBRT), Fosters Avenue, Dublin, Ireland. E-mail: weston.struwe@bioch.ox.ac.uk*

[b] *Fritz Haber Institute of the Max Planck Society, Faradayweg 4-6, 14195 Berlin, Germany. E-mail: baldauf@fhi-berlin.mpg.de*

[c] *Institut für Chemie und Biochemie der Freien Universität Berlin, Takustr. 3, 14195 Berlin, Germany. E-mail: kevin.pagel@fu-berlin.de*

[†] *Present address: University of Oxford, Department of Biochemistry, Oxford Glycobiology Institute, South Parks Road, OX1 3QU, Oxford, UK.*

- Supporting Information -

Materials. Lacto-*N*-neo-hexaose (LNnH: Gal(β1–4)GlcNAc(β1–6)(Gal(β1–4)GlcNAc(β13))Gal(β1–4)Glc) lacto-*N*-hexaose (LNH: Gal(β1–4)GlcNAc(β1–6)(Gal(β1–3)GlcNAc(β1–3))Gal(β1–4)Glc), lacto-*N*-tetraose (LNT: Gal(β1–3)GlcNAc(β1–3)Gal(β1–4)Glc) and lacto-*N*-neo-tetraose (LNnT: Gal(β1–4)GlcNAc(β1–3)Gal(β1–4)Glc) standards were purchased from Carbsynth Limited (Berkshire, UK). Human, horse and pig milk oligosaccharides were provided by Teagasc Food Research Centre (Fermoy, Ireland). Removal of sialic acid residues from human milk oligosaccharides was achieved by α2-3,6,8,9 neuraminidase A treatment (New England Biolabs, Ipswich, MA, USA). Oligosaccharide desalting was performed by porous graphitized carbon solid-phase extraction and cartridges were prepared in-house.

HPLC experiments.

2-aminobenzamide (2-AB) and HPLC grade solvents were purchased from Sigma Aldrich (Sigma, St. Louis, MO, USA). Fluorescent labelling and analysis was performed as described.[1] Briefly 20 µL 1% formic acid was added to dried aliquots of each milk oligosaccharide (100 nmol per reaction) and incubated for 40 minutes at room temperature. Samples were dried and 5 µL labelling solution containing 7:3 v/v DMSO/acetic acid, 1 M $NaCNBH_4$ and 0.5 M 2-AB was added and incubated at 65 °C overnight. Excess 2-AB was removed by normal phase retention using Phynexus DPA 65 resin tips. Dried samples were reconstituted in HPLC grade water prior to HILIC-HPLC analysis. HPLC was performed on an Alliance 2695 HPLC with a 2475 multi-wavelength fluorescence detector (Waters, Milford, MA, USA) with a TSK-Gel Amide-80, 5 µm 4.6 x 250 mm column (Tosoh Bioscience, Stuttgart, Germany). Solvent A was 50 mM formic acid adjusted to pH 4.4 with ammonia solution and solvent B was acetonitrile. Samples were injected in 80% acetonitrile and a linear gradient of 20–50% solvent A over 120 min at a flow rate of 0.4 mL/min was used. Data was collected with a fixed λ_{ex}=330 nm and λ_{em}=420 nm.

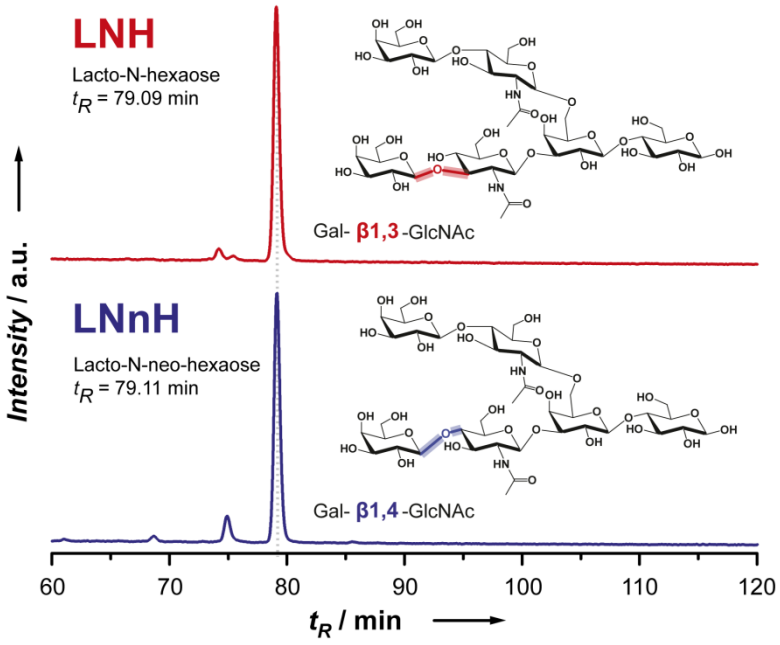

Fig. S1 Structures and HPLC chromatograms of the milk oligosaccharides LNH and LNnH. Both molecules have identical retention times and cannot be distinguished from one another.

IM-MS experiments. All samples were solved in water/methanol (1:1, *v:v*) at a concentration of 5-50 µM and measured individually at both positive and negative ion mode using ion mobility-mass spectrometry (IM-MS). In addition, equimolar mixtures of LNT/LNnT and LNH/LNnH were investigated. IM-MS and tandem MS (MS/MS) experiments were performed on a Synapt G2-S HDMS instrument (Waters, Manchester, UK),[2] which was mass calibrated prior to measurement using a solution of caesium iodide (100 mg·mL^{-1}). Typically 5 µL of sample were ionized using a nano-electrospray source (nESI) from platinum-palladium-coated borosilicate capillaries prepared in-house.[3] Instrument parameters were adjusted to produce predominantly singly charged ions and transmit them into the instrument (and especially into the IM cell) without extensive activation.[4, 5] Typical settings were: source temperature, 60 °C; needle voltage, 0.8 kV; sample cone voltage, 90 V; cone gas, 60 L/h. The ion mobility parameters values were: trap gas flow, 2 mL/min; helium cell gas flow, 180 mL/min; IMS gas flow, 120 mL/min; trap DC bias, 45 V; IMS wave velocity, 650 m/s; IMS wave height, 40 V. Data analysis was performed with MassLynx 4.1 and DriftScope 2.4 (Waters, Manchester, UK), and OriginPro 8.1 (OriginLab Corporation, Northampton).

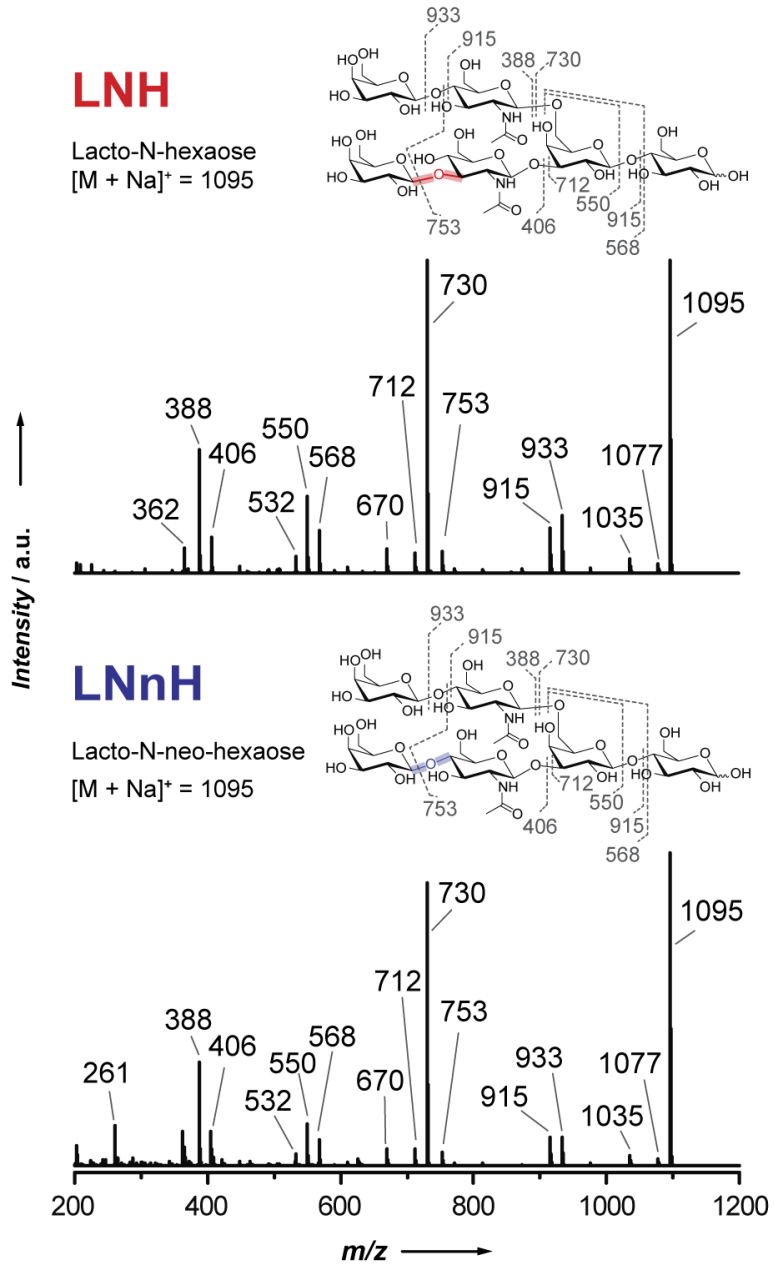

Fig. S2 Structures and tandem MS spectra of the milk oligosaccharides LNH and LNnH. Fragmentation spectra of $[M+Na]^+$ yield identical tandem MS spectra without diagnostic ions to differentiate both isomers.

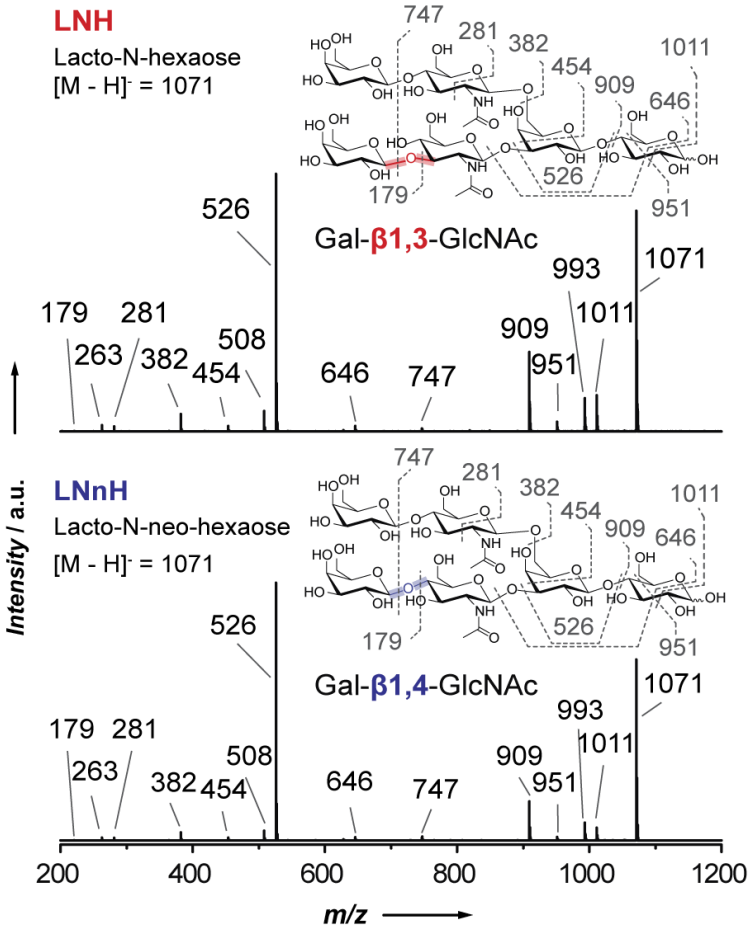

Fig. S3 Structures and tandem MS spectra of the milk oligosaccharides LNH and LNnH. Fragmentation of $[M-H]^-$ yields identical tandem MS spectra without diagnostic ions to differentiate the structures.

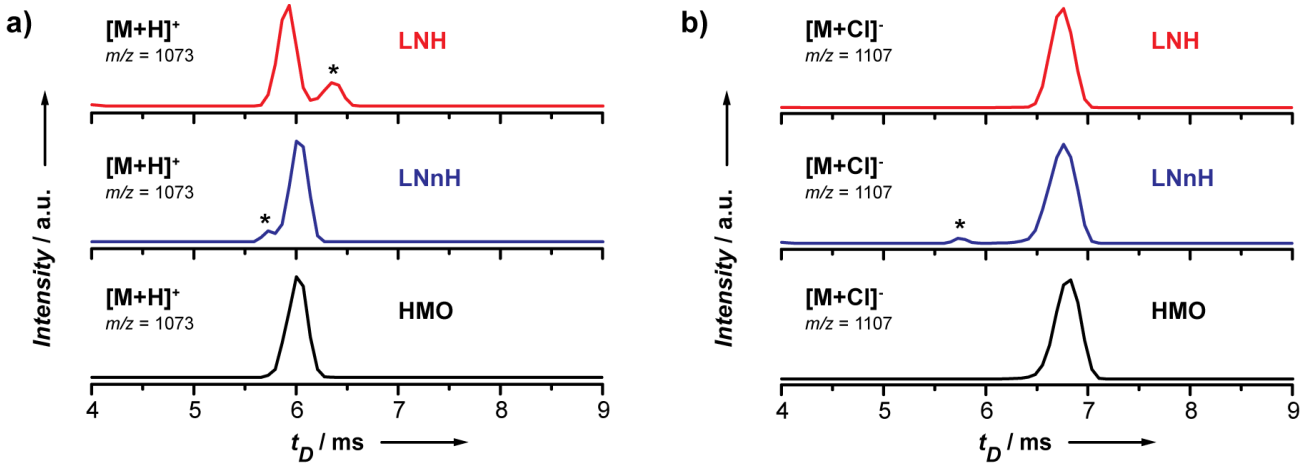

Fig. S4 Arrival time distributions of LNH (red), LNnH (blue), and human milk oligosaccharides (HMO; black) as a) $[M+H]^+$ and b) $[M+Cl]^-$ ions. The measurements were performed using nitrogen as drift gas. The asterisk indicates an impurity, which presumably stems from synthesis and was not observed in the biological samples

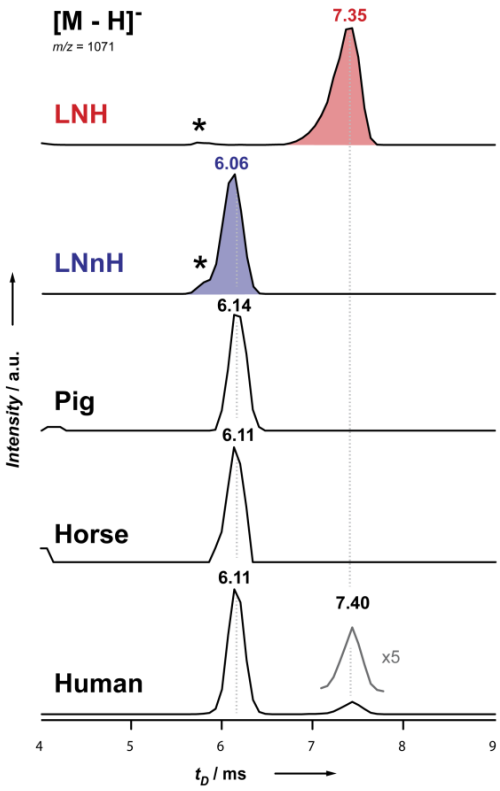

Fig S5 Arrival time distributions (ATDs) of deprotonated human milk oligosaccharides from different sources. The first two ATDs result from the synthetic LNH and LNnH and can be clearly distinguished based on their drift time t_D. The asterisk indicates an impurity presumably stemming from synthesis, which is not present in milk sugars extracted from pig, horse or human milk. Pig and horse milk show only the presence of LNnH while in human milk also LNH can be detected.

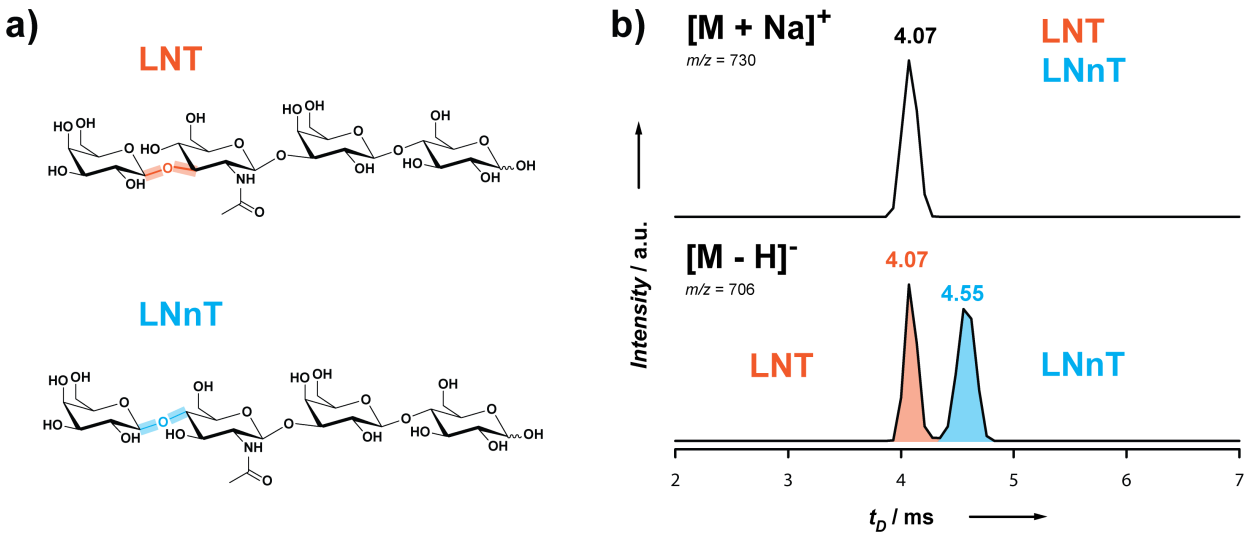

Fig. S6 IM-MS analysis of the milk sugars LNT and LNnT. a) Structures of lacto-N-tetraose (LNT) and lacto-N-neo-tetraose (LNnT). b) ATDs of an equimolar mixture of both oligosaccharides in positive and negative ion mode. $[M+Na]^+$ ions cannot be distinguished *via* IM-MS, while baseline separation is achieved for $[M-H]^-$ ions.

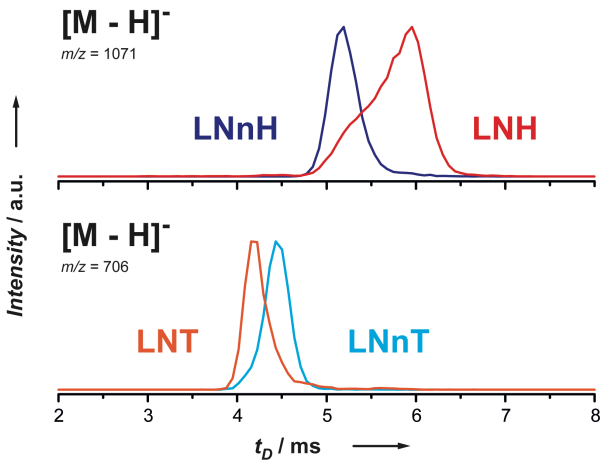

Fig. S7 ATDs of the milk sugars LNH, LNnH, LNT, and LNnT using helium as drift gas. Using a modified Synapt G2-S the drift times of the deprotonated milk sugars were measured in helium. The overall trend for their drift times remains the same compared to the measurements in nitrogen, however, due to a lower pressure in the drift cell (2.4 mbar) the difference of the drift times is smaller and the peaks are slightly broader.

CCS Measurements. CCSs were estimated according to a previously reported protocol using dextran as calibrant.[6, 7] Each sample was measured twice at five different wave velocities (450, 500, 550, 600, 650 m/s). Drift times t_D were extracted from raw data by fitting a Gaussian distribution to the arrival time distribution (ATD) of a given ion. A calibration curve for each wave velocity was generated considering only singly charged ions. All measurements were done using nitrogen as drift gas, however, by using helium CCS reference values for the calibration, pseudo helium CCSs ($^{TW}CCS_{He}$) could be estimated for the human milk oligosaccharides and are summarized in Table S1. This is possible, because the inverse mobilities of ions in helium and nitrogen are linearly correlated, as shown previously.[6, 7] CCSs values were deposited in the glycan IM database GlycoMob.[8]

Table S1 Estimated helium CCS of all investigated human milk oligosaccharides. CCSs are given in Å² with their respective double standard deviation (STD). STDs of synthetic samples were obtained of two independent replicates consisting each of measurements at five different wave velocities. STDs of biological HMO are calculated from measurements at five different wave velocities.

	$[M+H]^+$		$[M+Na]^+$		$[M-H]^-$		$[M+Cl]^-$	
	$^{TW}CCS_{He}$	STD	$^{TW}CCS_{He}$	STD	$^{TW}CCS_{He}$	STD	$^{TW}CCS_{He}$	STD
LNH	225.5	0.4	233.6	2.0	255.2	1.6	244.5	2.4
Human LNH	228.9	3.0	231.3	2.6	256.2	0.8	245.0	0.6
LNnH	228.6	1.0	225.0	2.0	227.6	1.8	244.3	1.2
Human LNnH	228.9	3.0	226.6	2.2	228.7	0.6	245.0	0.6
Pig LNnH	230.1	1.2	225.7	1.0	229.8	0.6	-	-
Horse LNnH	-	-	223.1	1.8	-	-	-	-
LNT	177.9	0.8	170.5	1.0	172.2	1.0	182.1	1.2
LNnT	189.1	0.4	169.6	1.0	186.3	0.8	180.4	0.8

Molecular Simulations. LNH and LNnH structures of the neutral and sodiated forms were generated by low-mode MD simulation using the Amber99 force field[9] with the software package MOE. Generated structures differed by a RMSD value of at least 0.15 Å and were considered if within an energy window of 126 kJ/mol. All structure candidates were subjected to geometry relaxations employing the PBE functional[10] corrected for long-range van der Waals interactions[11], first with *light* later with *tight* species defaults and computational settings[12]. Deprotonated forms were generated by individually removing each of the 18 hydroxy protons or of the 2 amide protons for the 40 lowest energy neutral conformers, yielding 660 starting structures for DFT relaxations. In case of LNnH, this was performed for the open chain form and the β-anomer of the reducing end sugar (data not shown). Energy hierarchies shown in the manuscript refer to PBE+vdW energies computed with a tier-2 basis set and tight computational settings. Collision cross sections were calculated based on the PBE+vdW conformers with the projection approximation method; similar trends were also observed using the trajectory method (TM)[13] optimized for the drift gas nitrogen (Figure S9).[14] For selected conformers of deprotonated LNnH, DFT MD simulations were performed for about 8 ps each with the Bussi-Donadio-Parrinello thermostat[15] at 330 K. One of the trajectories was extended to 20 ps in order to illustrate the mobile protons (see attached movie).

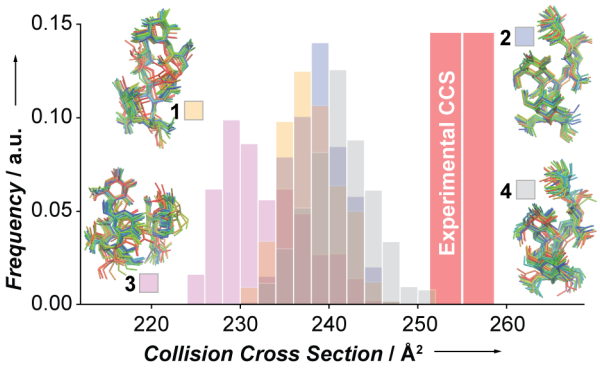

Fig. S8 Distribution of theoretical CCSs of four representative low energy structures of LNH from *ab initio* MD simulations. For comparison, the experimental CCS is given as a red bar with a width representing a typical error of 1.5%. Large fluctuations in theoretical CCS are observed for the four times 8 ps simulation time.

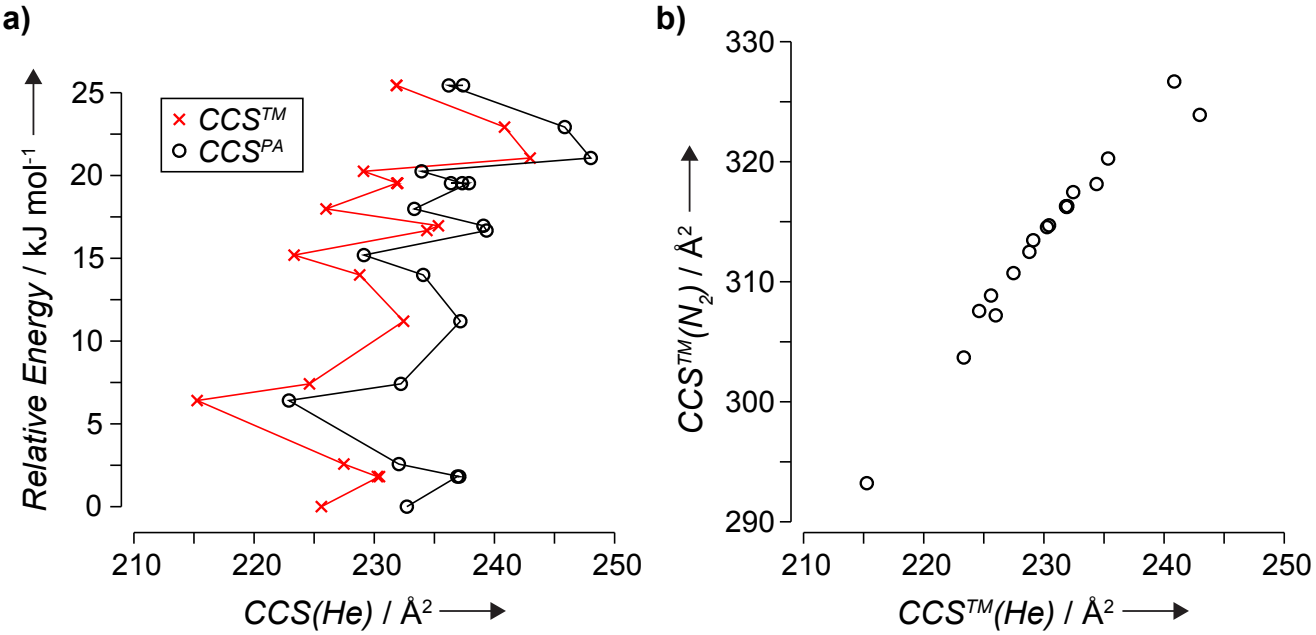

Fig. S9. Comparison of calculated collision cross sections (CCSs) computed for the 20 lowest energy conformers of deprotonated LNH using different methods. a) Relative energies at the PBE+vdW level plotted against CCS computed with the projection approximation (CCS^{PA}) and with the trajectory method (CCS™). The connecting lines only serve as a guide to the eye. b) CCS values calculated with the trajectory method for the buffer gases N_2 and He.

References

1 W. B. Struwe and P. M. Rudd, *Biol. Chem.*, 2012, **393**, 757-765.

2 S. D. Pringle, K. Giles, J. L. Wildgoose, J. P. Williams, S. E. Slade, K. Thalassinos, R. H. Bateman, M. T. Bowers and J. H. Scrivens, *Int. J. Mass Spectrom.*, 2007, **261**, 1-12.

3 H. Hernandez and C. V. Robinson, *Nat. Protoc.*, 2007, **2**, 715-726.

4 S. I. Merenbloom, T. G. Flick and E. R. Williams, *J. Am. Soc. Mass Spectrom.*, 2012, **23**, 553-562.

5 D. Morsa, V. Gabelica and E. De Pauw, *Anal. Chem.*, 2011, **83**, 5775-5782.

6 K. Pagel and D. J. Harvey, *Anal. Chem.*, 2013, **85**, 5138-5145.

7 J. Hofmann, W. B. Struwe, C. A. Scarff, J. H. Scrivens, D. J. Harvey and K. Pagel, *Anal. Chem.*, 2014, **86**, 10789-10795.

8 W. B. Struwe, K. Pagel, J. L. P. Benesch, D. J. Harvey and M. P. Campbell, *Glycoconj. J.*, 2016, **33**, 399-404.

9 J. Wang, P. Cieplak and P. A. Kollman, *J. Comput. Chem.*, 2000, **21**, 1049-1074.

10 J. P. Perdew, K. Burke and M. Ernzerhof, *Phys. Rev. Lett.*, 1996, **77**, 3865-3868.

11 A. Tkatchenko and M. Scheffler, *Phys. Rev. Lett.*, 2009, **102**, 073005.

12 V. Blum, R. Gehrke, F. Hanke, P. Havu, V. Havu, X. Ren, K. Reuter and M. Scheffler, *Comput. Phys. Commun.*, 2009, **180**, 2175-2196.

13 M. F. Mesleh, J. M. Hunter, A. A. Shvartsburg, G. C. Schatz and M. F. Jarrold, *J. Phys. Chem.*, 1996, **100**, 16082-16086.

14 I. Campuzano, M. F. Bush, C. V. Robinson, C. Beaumont, K. Richardson, H. Kim and H. I. Kim, *Anal. Chem.*, 2012, **84**, 1026-1033.

15 G. Bussi, D. Donadio and M. Parrinello, *J. Chem. Phys.*, 2007, **126**, 014101.